Effect of operating conditions on core noise for a realistic gas-turbine combustor

By C. X. Shao AND M. Ihme

1. Motivation and objectives

Civil aircraft will continue to transport people for decades to come. However, aircraft noise is a major issue because it adversely impacts humans' physical and psychological health (Basner *et al.* 2017) and constrains the growth of air traffic. The International Civil Aviation Organization has issued Annex-16 in order to counter aircraft noise pollution. NASA has proposed an ambitious noise reduction goal (NASA 2002) reducing the perceived aircraft noise levels by three-quarters in 25 years.

It is well established that the main contributors to aircraft noise are airframe and engine noise (Ihme 2017). Airframe noise is generated by the trailing edge, landing gear, and wings. Engine noise is generated by the fan, compressor, combustor, turbine, and jet exhaust. In particular, engine-core noise refers to the noise generated by the combustor and turbine sections.

Engine-core noise is attracting more and more attention. On one hand, in order to reduce nitrogen oxide and greenhouse gas emissions, advanced combustion technologies such as lean combustion and lean premixed pre-vaporized combustion are commonly employed. Such lean combustion could generate louder noise since it is sensitive to the unsteady turbulent environment of the combustion chamber (Liu *et al.* 2013; Dowling & Mahmoudi 2015). On the other hand, fan and jet noise has been largely reduced by using a high bypass ratio in turbofan engines as well as better fan blade geometric design, acoustic liners, and nozzle design (Magri *et al.* 2018; Pillai & Kurose 2018). Engine-core noise is thus a relatively important cause of noise pollution generated by the entire aircraft.

Engine-core noise could be caused by direct noise or indirect noise (Candel *et al.* 2009; Dowling & Mahmoudi 2015; Ihme 2017). Direct combustion noise describes the transmission of pressure fluctuations originating from unsteady heat release in the combustion chamber (Candel *et al.* 2009). The sound generated by direct combustion noise could be transmitted to the downstream components and result in noise pollution, whereas the noise that is reflected at the nozzle could result in thermoacoustic instability (Lieuwen 2012). Indirect combustion noise is caused by the convection of unsteady vortices and entropy variations by temperature hot spots as they propagate from the combustor to the downstream turbine and nozzle (Marble & Candel 1977). Contributions from mixture inhomogeneities have recently been identified as an additional source of indirect combustion noise that so far has not been considered (Ihme 2017; Magri *et al.* 2016).

With increasing computational resources, multidimensional numerical simulations have been employed to investigate core noise (Ihme 2017). Leyko *et al.* (2009) compared direct and indirect noise mechanisms in a model combustor and found that indirect noise is small in laboratory experiments but increases in more realistic aeronautical engines. By using large-eddy simulation (LES), Papadogiannis *et al.* (2016) assessed entropy noise generated in a high-pressure turbine stage and found that the upstream entropy noise

was reduced due to the choked turbine nozzle guide vane. O'Brien *et al.* (2015) used a hybrid modeling approach to predict the core noise from a system that consists of combustor, turbine, nozzle, and far-field radiation. Livebardon *et al.* (2016) combined LES and actuator disk theory to predict combustion noise in a helicopter engine, confirming the importance of indirect combustion noise. Recently, Ihme *et al.* (2017) employed a hybrid model consisting of unsteady combustor LES and a reduced-order model of the nozzle flow. The results showed that non-compact nozzle theory is necessary to capture phase-cancellation effects, and the complex mode shapes of the perturbations entering the nozzle should be considered. Magri *et al.* (2018) numerically calculated the indirect noise for Helmholtz numbers up to 2 in nozzles with a linear velocity profile and found that the compositional noise can be at least as large as the direct noise and entropy noise in choked nozzles and lean mixtures. Giusti *et al.* (2019) investigated indirect noise in a realistic rich-quench-lean (RQL) combustor coupled with a nozzle guide vane and found that entropy noise is larger than compositional noise. By simulating a realistic combustor for an aero engine application, Motheau *et al.* (2014) found that combustion instability around the characteristic frequency stems from a mixed acoustic-entropy mode. Pillai & Kurose (2018) investigated the combustion noise of a turbulent spray flame using a hybrid direct numerical simulation and computational aero acoustics approach, and they found that the acoustic power spectra exhibit a power law dependence of the form $f^{-2.4}$ (where f is the frequency) in the low frequency.

These computational investigations have shown that the relative contribution of direct and indirect noise to the overall core-noise radiation has not been fully revealed. Here are the questions for different operating conditions: Are the noise sources different for different conditions? Which noise source contributes most under different operating conditions? To this end, the objective of this work is to investigate the relative importance of core-noise sources in a realistic gas-turbine combustor operated in lean blowout conditions, and the focus is on the effects of cruise and take-off conditions. The experimental configuration and operating conditions are presented in Section 2. Results are discussed in Section 3, and conclusions are provided in Section 4.

2. Experimental configuration and operating conditions

2.1. *Experimental configuration*

The referee combustor rig that is considered in this study was designed to reproduce features of a realistic RQL gas-turbine combustor (Stouffer *et al.* 2017; Colket *et al.* 2016). Shao *et al.* (2020) presents a schematic of this combustor. The combustor consists of four components, namely the pressure plenum, the injector, the combustion chamber, and the outlet plenum. The injector consists of an inner radial swirler and two outer axial swirlers that supply air to the combustion chamber. Fuel is supplied through a pressure-swirl atomizer at the center. The combustion chamber has a constant width of 110 mm in the primary and secondary combustion regions, and progressively reduces in the dilution zone until the exhaust. The upper and lower walls of the combustor consist of multi-perforated plates that supply air from the pressure plenum to the combustion chamber. There are two rows of dilution holes in the upper and lower walls of the chamber. The first row consists of three dilution holes on each side and is located 45 mm downstream of the injection plane, and the second row consists of four dilution holes on each side and is 132 mm downstream of the injection plane. The combustion chamber is housed

inside a pressure plenum. Other geometric details are provided by Stouffer *et al.* (2017) and Esclapez *et al.* (2017).

2.2. *Operating conditions*

The present study considers a conventional petroleum-derived Jet A fuel (POSF10325). The thermo-physico-chemical properties of this fuel are obtained from studies conducted by the National Jet Fuel Combustion Program (Colket *et al.* 2016), and the kinetic model describing the reaction chemistry uses the HyChem approach (Wang *et al.* 2018). The properties of the liquid fuel are dependent on the temperature, and the effects of pressure are negligible.

To examine the effect of the operating conditions on noise emission, we consider two different operating points, corresponding to cruise and take-off conditions. For the cruise condition, the aircraft is assumed to be flying at an altitude of 35,000 ft with a flight Mach number of 0.8. The combustor is operated at approximately 20% of the maximum take-off power (Jenkinson *et al.* 1999). The conditions of this operation point are identical to those considered in an experimental study of the same combustor rig (Monfort *et al.* 2017). The combustor is supplied with air at a temperature of 394 ± 2.5 K, and the total air mass flow rate is 391.4 ± 6.9 g/s. The pressure inside the combustion chamber is 2.07 ± 0.01 atm. The fuel is supplied through a pressure-swirl atomizer at 322 ± 2.3 K, and the mass flow rate is 4.0 g/s with an uncertainty of 0.15%. The overall equivalence ratio is $\phi_g = 0.15$.

The take-off operating point is specified by considering sea-level conditions. The parameters for the take-off condition, i.e., mass flow rates and combustion pressure, are determined by considering a typical turbo-fan engine that consists of a fan, compressor, combustor, turbine, and nozzle. The thrust generated by a high bypass ratio turbofan engine is determined as (Mattingly & Boyer 2016)

$$F = \dot{m}_C \left[(1 + f_r)U_9 + \beta U_{19} - (1 + \beta)U_0\right] + A_9 \left(p_9 - p_0\right) + A_{19} \left(p_{1e} - p_0\right), \tag{2.1}$$

where $\dot{m}_C$ is the air mass flow rate through the core, f_r is the fuel-air ratio, β is the bypass ratio, U_9 and U_{19} are the core exit velocity and fan exit velocity, U_0 is the flight velocity, p_9 and p_0 are the static pressure at the jet nozzle and at the ambient environment, and A_9 and A_{19} are the cross sections of the core and the fan, respectively. Assuming perfectly expanded nozzle flow, the pressure thrust in Eq. (2.1) is neglected, and the operating parameters for the take-off conditions are then determined from an ideal Brayton-cycle analysis (Mattingly & Boyer 2016). To anchor the operating point in relation to the cruise condition, we prescribe the fan pressure ratio and bypass ratio from a CFM56 high-bypass-ratio turbofan engine (El-Sayed 2008), i.e., $\pi_f = 1.28$ and $\beta = 6.6$. All other parameters for the combustor pressure, fuel mass flow rate, and equivalence ratio are then computed subject to prescribed conditions for flight Mach number M_0, ambient temperature T_0, ratio of specific heats γ, heat capacity c_p, lower heating value Δh, temperature at the combustor exit T_{t4}, compressor pressure ratio π_c, fan pressure ratio π_f, and bypass ratio β. The temperature at the combustor exit is determined iteratively to obtain a reasonable compressor pressure ratio for cruise and take-off conditions. The operating parameters for both conditions are summarized in Table 1.

2.3. *Hybrid method*

A hybrid model is developed to predict the generation and transmission of engine-core noise in a realistic combustor-nozzle configuration. In this hybrid approach, compressible reacting multiphase LES is employed to describe the turbulent combustion. The

Parameters	Cruise	Take-off
M_0 (none)	0.8	0.0
π_c (none)	5.71	9.56
$\dot{m}_C$ (g/s)	391.4	765.2
T_3 (K)	394.0	549.3
T_{t4} (K)	837.4	1349.5
V_9 (m/s)	464.76	695.33
$F/\dot{m}_0$ [N/(kg/s)]	87.91	269.52
ϕ_g (none)	0.15	0.28
p_c (atm)	2.07	10.35
M_9 (none)	1.09	1.31
τ_c (none)	1.645	1.906
$\dot{m}_f$ (g/s)	4.0	14.2
T_f (K)	322.0	322.0
f_r (none)	0.01	0.01856
$TSFC$ (mg/s/N)	14.97	9.06
F (N)	261.22	1567.32
d_{SMD} (μm)	56.0	14.5

TABLE 1. Operating parameters for cruise and take-off conditions. M_0: flight Mach number, π_c: compressor pressure ratio, $\dot{m}_C$: air mass flow rate through the core, T_3: air temperature entering the combustor, T_{t4}: combustor exit temperature, V_9: core nozzle exit velocity, $F/\dot{m}_0$: specific thrust, ϕ_g: global equivalence ratio, p_c: pressure in the combustor, M_9: Mach number at core nozzle exit, τ_c: temperature ratio of compressor, $\dot{m}_f$: fuel mass flow rate, T_f: fuel temperature at injection, f_r: fuel-air ratio, $TSFC$: thrust-specific fuel consumption, F: thrust, d_{SMD}: Sauter mean diameter.

unsteady flow field at the combustor exit is then extracted from the LES and used as the inflow boundary condition for a reduced-order nozzle simulation using the linearized Euler equations (LEE). The nozzle is represented by a converging-diverging supersonic nozzle. The details of the method are given by Shao *et al.* (2020).

3. Results

To evaluate the strengths of the acoustic sources, we begin our acoustic analysis by investigating results from one-dimensional counterflow diffusion flames. These calculations are performed using FlameMaster (Pitsch 1998). Profiles of temperature and species mass fractions for cruise and take-off conditions at stoichiometric scalar dissipation rates of $\chi_{st} = 1\,\mathrm{s}^{-1}$ and $50\,\mathrm{s}^{-1}$ are shown in Figure 1. The lower dissipation rate is representative of the cruise condition at the combustor exit, while the higher rate is representative of the take-off condition. Figure 1 compares the flame structures in both operating conditions, showing similar profiles for temperature and major species. This is in agreement with findings by Sun *et al.* (1996), who investigated the structure of diffusion flames at elevated pressure. The mean composition at the combustor exit corresponds to a mean-flow composition of $\langle Z \rangle = 0.013$, which corresponds to $Z(1 + Z_{st})/(Z + Z_{st}) = 0.17$ (see the dashed vertical lines in Figure 1). For this condition, the overall mass fractions of the major species (N_2, O_2, CO_2, H_2O, CO) amount to 99.99 % of the composition, which is used to evaluate the chemical potential function.

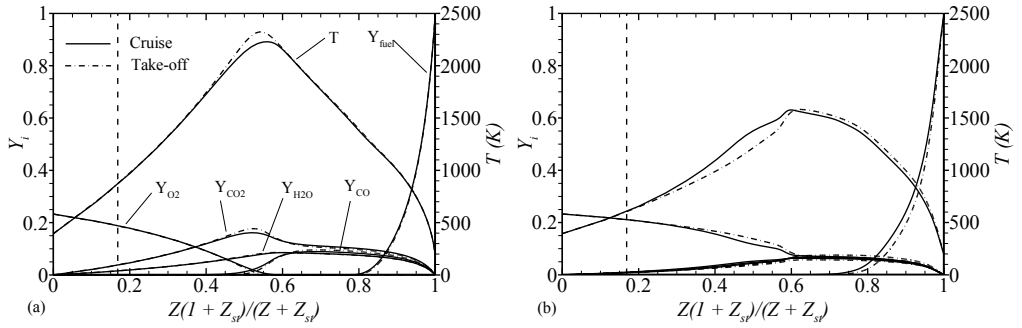

FIGURE 1. One-dimensional POSF10325-air counterflow diffusion flame for a scalar dissipation rate of $\chi_{st} = 1\,\mathrm{s}^{-1}$ (a) and $\chi_{st} = 50\,\mathrm{s}^{-1}$ (b). The vertical dashed lines indicate the condition of global equivalence ratio.

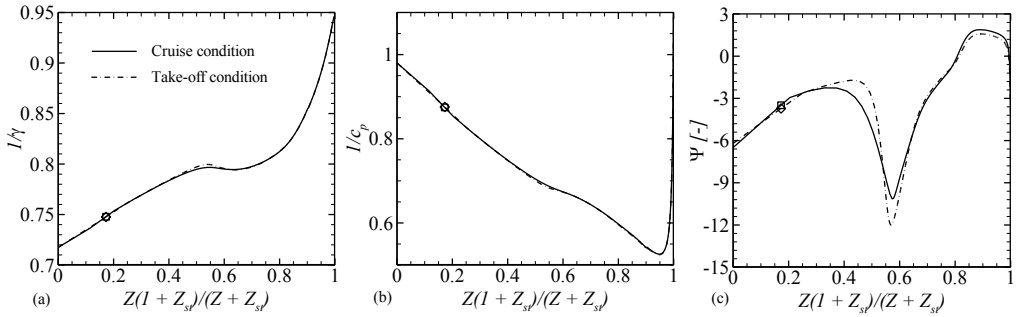

FIGURE 2. Strengths of sources for acoustic (a), entropy (b) and compositional (c) noise at cruise and take-off conditions. The symbols represent the conditions in this work.

The noise transmission through the nozzle and its emission are affected by two aspects. One is the perturbation of the flow-field quantities exiting the combustor and entering the nozzle, i.e., p', u', s', and Z'. These fluctuations are determined by combustor operation and can be characterized by the spectra. The second aspect arises from the nozzle-flow and thermodynamic properties that characterize the acoustic sources, namely the heat capacity c_p and the chemical potential function Ψ. The coefficients γ^{-1}, c_p^{-1}, and Ψ determine the source strength for acoustic, entropy, and compositional noise, respectively (Ihme 2017). These quantities are depicted in Figure 2 as a function of mixture fraction, showing that the strengths of the noise sources have negligible differences between cruise and take-off conditions. This is attributed to the fact that the composition of the mixture is nearly identical at the combustor exit for these two conditions, suggesting that the noise differences between cruise and take-off conditions largely arise from differences in the combustor exit conditions. Figure 2 shows that Ψ has an opposite sign to the entropy fluctuation, s'/c_p, for fuel-lean mixtures. This difference will affect the phase between entropy and compositional noise.

While Figure 2 presents the overall strengths of the noise sources as a function of mixture fraction, it offers little explanation as to how the difference between species gives rise to the noise. Species contributions to the strengths of direct and entropy noise can be directly determined from Figure 1 since c_p is determined from the mixture composition: $c_p = \sum_{i=1}^{N_s} c_{p,i} Y_i$. Specifically, for a lean-mixture composition the main contribution to

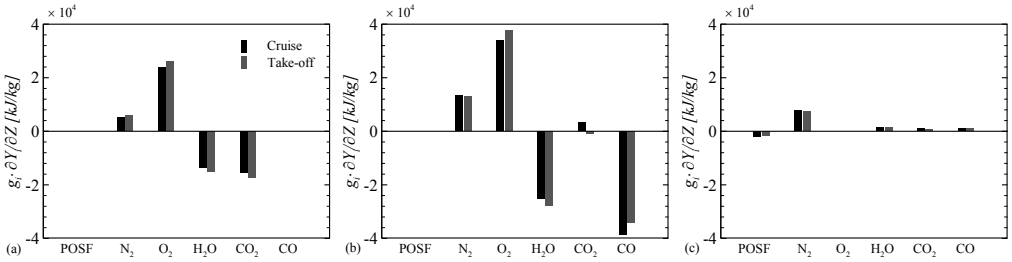

FIGURE 3. Contribution of the dominant species to the chemical potential function, Ψ, i.e., $g_i \partial Y_i / \partial Z$ at different mean mixture fractions, where the lean mixture corresponds to the present combustor exit condition.

entropy and compositional noise arises from O_2, H_2O, N_2, and CO_2. It is the difference in Gibbs free energy g_i and species gradients $\partial_Z Y_i$ that induce changes in the chemical potential function and the compositional noise.

To understand the sensitivity of compositional noise to individual species, the contributions of the dominant species to the chemical potential function are examined for three different mixture compositions. The results are presented in Figure 3, showing that the acoustically most effective species depend on the mixture composition. Specifically, for lean mixtures that are representative of the present combustor exit condition, O_2, H_2O, and CO_2 are the main contributors to the compositional noise. However, none of these species contributes to the compositional noise at rich conditions. For the stoichiometric mixture, the intermediate species CO is the main contributor to the chemical potential. This analysis indicates that the mixture composition requires consideration in the analysis of indirect combustion noise, and measurements of major species (O_2, H_2O, CO_2) are useful to guide theoretical analysis.

We proceed by examining the relative importance of core-noise sources. We consider the noise emission at frequencies between 200 and 1400 Hz. The nozzle length is 0.5 m, and the Mach number at the nozzle exit is 1.5. Nozzle-inflow conditions are prescribed by a harmonic function: $q'(y,t) = \psi_1(y)\sin(2\pi f_c t + \phi_q)$, with $\phi_q = \{0, -\pi/2, \pi/2, \pi/2\}$ for $q = \{p, u, s, Z\}$. The phase shift is computed from the Fast Fourier Transform of signals at the combustor exit. The amplitudes are extracted from the spectra, and the discrete frequencies considered are $f_c = \{254, 506, 760, 876, 1000, 1344\}$ Hz for the cruise and take-off conditions. The planar mode shape along the y direction is used for all frequencies.

Sound pressure levels for direct and indirect noise emissions at the nozzle exit are presented in Figure 4. These results show that the sound pressure level predicted for the take-off condition is $\sim$ 10–20 dB higher than in the cruise condition for both direct and indirect noise. Regarding the relative noise source contributions, the entropy noise and compositional noise exceed the direct noise at frequencies below $\sim$ 200–600 Hz for both conditions. For indirect noise, the contribution from compositional noise is 10 dB higher than entropy noise for both conditions. These predictions imply that compositional noise is the most dominant source and that entropy noise is secondary for noise emission. From the relative contribution of each noise source, we further notice that a phase shift between entropy noise and compositional noise leads to cancellation of indirect noise sources. This is also consistent with previous findings (Shao *et al.* 2020) under fuel-lean conditions. Mathematically, this is attributed to the fact that the chemical potential

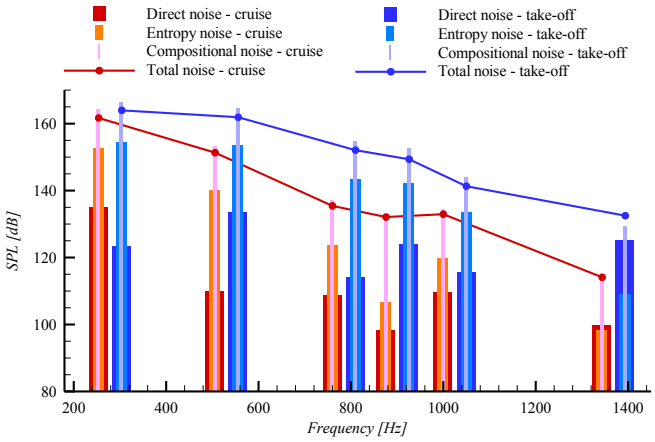

FIGURE 4. Sound pressure levels for direct and indirect noise predicted by LEE simulations for the cruise and take-off conditions. The red and blue lines/bars denote cruise and take-off conditions, respectively.

function is negative for a fuel-lean mixture, which is opposite to the strength of the entropy noise, as shown in Figure 2.

4. Conclusions

In this study, combustion noise in a realistic gas-turbine combustor was investigated using a hybrid LES/LEE framework. The formation and evolution of direct and indirect noise were investigated, and the relative importance of noise sources for two distinct operating points was examined. The following conclusions can be drawn.

The strength of the noise sources and the degree of fluctuations at the combustor exit are the two main reasons for the noise emission at the nozzle exit. The relative strengths of the noise sources are comparable for cruise and take-off conditions, while the degree of fluctuations at the combustor exit is significantly higher under take-off conditions. This, in turn, suggests that for the present combustor configuration the relevant contributions of direct and indirect noise remain the same, regardless of operating conditions. The species O_2, H_2O, N_2, and CO_2 are the primary contributors to the indirect noise arising from mixture inhomogeneities under fuel-lean conditions. The direct and indirect noises are $\sim$ 10–20 dB higher for the take-off condition, and the compositional noise exceeds the temperature-induced entropy noise.

Acknowledgments

This investigation was funded by the Aero-acoustics Research Consortium grant OAI-AARCS-19026. The computational resources supporting this work were provided by the NASA Advanced Supercomputing (NAS) Division at Ames Research Center and National Energy Research Scientific Computing Center (NERSC). We thank Dr. Jeonglae Kim for sharing the LEE solver and Danyal Mohaddes for fruitful discussions on the combustion analysis.

REFERENCES

Basner, M., Clark, C., Hansell, A., Hileman, J. I., Janssen, S., Shepherd, K. & Sparrow, V. 2017 Aviation noise impacts: State of the science. *Noise Health* **19**, 41–50.

Candel, S., Durox, D., Ducruix, S., Birbaud, A.-L., Noiray, N. & Schuller, T. 2009 Flame dynamics and combustion noise: progress and challenges. *Int. J. Aeroacoust.* **8**, 1–56.

Colket, M. *et al.* 2016 An overview of the national jet fuels combustion program. *AIAA Paper* pp. 2016–0177.

Dowling, A. P. & Mahmoudi, Y. 2015 Combustion noise. *P. Combust. Inst.* **35**, 65–100.

El-Sayed, A. F. 2008 *Aircraft Propulsion and Gas Turbine Engines*. CRC Press.

Esclapez, L., Ma, P. C., Mayhew, E., Xu, R., Stouffer, S., Lee, T., Wang, H. & Ihme, M. 2017 Fuel effects on lean blowout in a realistic gas turbine combustor. *Combust. Flame* **181**, 82–99.

Giusti, A., Magri, L. & Zedda, M. 2019 Flow inhomogeneities in a realistic aeronautical gas-turbine combustor: formation, evolution, and indirect noise. *J. Eng. Gas Turb. Power* **141**, 011502.

Ihme, M. 2017 Combustion and engine-core noise. *Annu. Rev. Fluid Mech.* **49**, 277–310.

Ihme, M., O'Brien, J. & Kim, J. 2017 Compositional inhomogeneities as a source of indirect combustion noise: physical mechanisms and fuel effects. *the 24th International Congress on Sound and Vibration* .

Jenkinson, L., Simpkin, P. & Rhodes, D. 1999 *Civil Jet Aircraft Design*. American Institute of Aeronautics and Astronautics.

Leyko, M., Nicoud, F. & Poinsot, T. 2009 Comparison of direct and indirect combustion noise mechanisms in a model combustor. *AIAA J.* **47**, 2709–2716.

Lieuwen, T. C. 2012 *Unsteady Combustor Physics*. Cambridge University Press.

Liu, Y., Dowling, A., Swaminathan, N., Morvant, R., Macquisten, M. & Caracciolo, L. 2013 Prediction of combustion noise for an aeroengine combustor. *J. Propul. Power* **30**, 114–122.

Livebardon, T., Moreau, S., Gicquel, L., Poinsot, T. & Bouty, E. 2016 Combining les of combustion chamber and an actuator disk theory to predict combustion noise in a helicopter engine. *Combust. Flame* **165**, 272–287.

Magri, L., O'Brien, J. & Ihme, M. 2016 Compositional inhomogeneities as a source of indirect combustion noise. *J. Fluid Mech.* **799**, R4.

Magri, L., O'Brien, J. & Ihme, M. 2018 Effects of nozzle Helmholtz number on indirect combustion noise by compositional perturbations. *J. Eng. Gas Turb. Power* **140**, 1–9.

Marble, F. E. & Candel, S. M. 1977 Acoustic disturbance from gas non-uniformities convected through a nozzle. *J. Sound Vib.* **55**, 225–243.

Mattingly, J. D. & Boyer, K. M. 2016 *Elements of Propulsion: Gas Turbines and Rockets*. American Institute of Aeronautics and Astronautics.

Monfort, J. R., Stouffer, S. D., Hendershott, T. H., Wrzesinski, P. J., Foley, W. S. & Rein, K. D. 2017 Evaluating combustion instability in a swirl-stabilized combustor using simultaneous pressure, temperature, and chemiluminescence measurements at high repetition rates. *AIAA Paper* pp. 2017–1101.

Motheau, E., Nicoud, F. & Poinsot, T. 2014 Mixed acoustic–entropy combustion instabilities in gas turbines. *J. Fluid Mech.* **749**, 542–576.

NASA 2002 NASA's Quiet Aircraft Technology Program. *FS-2002-09-73-LaRC* .

O'Brien, J., Kim, J. & Ihme, M. 2015 Integrated analysis of jet-engine core noise using a hybrid modeling approach. *AIAA Paper* pp. 2015–2821.

Papadogiannis, D., Wang, G., Moreau, S., Duchaine, F., Gicquel, L. & Nicoud, F. 2016 Assessment of the indirect combustion noise generated in a transonic high-pressure turbine stage. *J. Eng. Gas Turb. Power* **138**, 1–8.

Pillai, A. & Kurose, R. 2018 Combustion noise analysis of a turbulent spray flame using a hybrid DNS/APE-RF approach. *Combust. Flame* **200**, 168–191.

Pitsch, H. 1998 FlameMaster v3.1: A C++ computer program for 0D combustion and 1D laminar flame calculations.

Shao, C., Maeda, K. & Ihme, M. 2020 Analysis of core-noise contributions in a realistic gas-turbine combustor operated near lean blow-out. *P. Combust. Inst.* DOI: 10.1016/j.proci.2020.07.078.

Stouffer, S., Hendershott, T., Monfort, J. R., Diemer, J., Corporan, E., Wrzesinski, P. & Caswell, A. W. 2017 Lean blowout and ignition characteristics of conventional and surrogate fuels measured in a swirl stabilized combustor. *AIAA Paper* pp. 2017–1954.

Sun, C. J., Sung, C. J., Zhu, D. L. & Law, C. K. 1996 Response of counterflow premixed and diffusion flames to strain rate variations at reduced and elevated pressures. *Symp. (Int.) Combust.* **26**, 1111–1120.

Wang, H., Xu, R., Wang, K., Bowman, C. T., Davidson, D. F., Hanson, R. K., Brezinsky, K. & Egolfopoulos, F. N. 2018 A physics-based approach to modeling real-fuel combustion chemistry. I. Evidence from experiments, and thermodynamic, chemical kinetic and statistical considerations. *Combust. Flame* **193**, 502–519.